ISSN 1063-7761, Journal of Experimental and Theoretical Physics, 2018, Vol. 126, No. 4, pp. 497–505. © Pleiades Publishing, Inc., 2018.
Original Russian Text © A.V. Nemtsev, V.S. Zhandun, V.I. Zinenko, 2018, published in Zhurnal Eksperimental'noi i Teoreticheskoi Fiziki, 2018, Vol. 153, No. 4, pp. 597–606.

ORDER, DISORDER, AND PHASE TRANSITION IN CONDENSED SYSTEM

Ab Initio Study of the Polarization, Electronic, Magnetic, and Optical Properties of Perovskite $SrMO_3$ (M = Fe, Mn) Crystals and Thin Films Containing Magnetic Ions

A. V. Nemtsev[a], V. S. Zhandun[a,*], and V. I. Zinenko[a]

[a] *Kirensky Institute of Physics, Siberian Branch, Russian Academy of Sciences, Krasnoyarsk, 660036 Russia*

**e-mail: jvc@iph.krasn.ru*

Received October 12, 2017

Abstract—The magnetic, electronic, and polarization properties of the $SrFeO_3$ and $SrMnO_3$ compounds with a perovskite structure are calculated using the density functional theory in the bulk and thin-film states. A ferroelectric instability is found to be absent in the bulk state, and the polar mode is softened in the thin-film state of $SrMnO_3$ in the presence of tensile stresses in the substrate. As a result, a polar phase with a polarization of 23 $\mu C/cm^2$ appears, which agrees with experimental data. The study of the magnetic and electronic properties demonstrates the existence of *G*-type antiferromagnetic ordering in $SrMnO_3$ and the appearance of a dielectric gap of about 1.5 eV in its thin film. A ferromagnetic phase with metallic conduction in both the bulk and thin-film states is detected in $SrFeO_3$.

DOI: 10.1134/S1063776118030056

1. INTRODUCTION

Perovskite-based compounds belong to the class of functional materials due to the variety of their properties, including ferroelectric and magnetoelectric ones. Ferroelectric crystals with an ABO_3 perovskite structure have been experimentally and theoretically studied for more than 70 years. These compounds are characterized by a simple structure and, on the other hand, various compositions, which include almost all elements from the periodic table. Therefore, using experimental and theoretical methods, researchers revealed a variety of functional properties (magnetic, optical, electronic, ferroelectric, magnetoelectric properties), which can have a wide spectrum of practical application [1–5]. Although a large number of perovskite-based ferroelectric and magnetic compounds exists, researchers continue to synthesize new perovskites with interesting physicochemical properties, which attract keen interest from both fundamental and applied standpoints due to fresh possibilities of their application [6, 7]. For example, the presence of switchable spontaneous polarization is the basis for creating random-access memory, the high permittivity of ferroelectrics makes them promising for replacing silicon in field-effect semiconductor transistor, their piezoelectric properties can be used to apply perovskites as transducers in various types of detectors, and the existence of magnetic ions in their structure leads to the possibility of application of their magnetic and electronic properties in spintronics [8–10]. One of the modern problems that prevent the development of spintronic memory devices is the necessity of high currents for data recording using the effect of changing a magnetization direction. One of the methods for solving this problem is the use of magnetoelectric materials, where an applied electric field can change magnetization.

On the other hand, the development of modern technologies needs miniature materials for modern nanotechnological devices. The decrease in the dimension of a crystal from a bulk to a thin-film state significantly changes the physical properties of compounds, up to the appearance of new advanced properties of materials. In the recent decades, this finding has stimulated an active investigation of the physical properties, including the ferroelectric and magnetoelectric properties, of thin films 1–10 nm thick [11–13].

The $SrTiO_3$ compound is one of the well-known and most extensively studied compounds with a perovskite structure. The ferroelectric instability is absent in this compound down to low temperatures [14, 15], and the appearance of spontaneous polar-

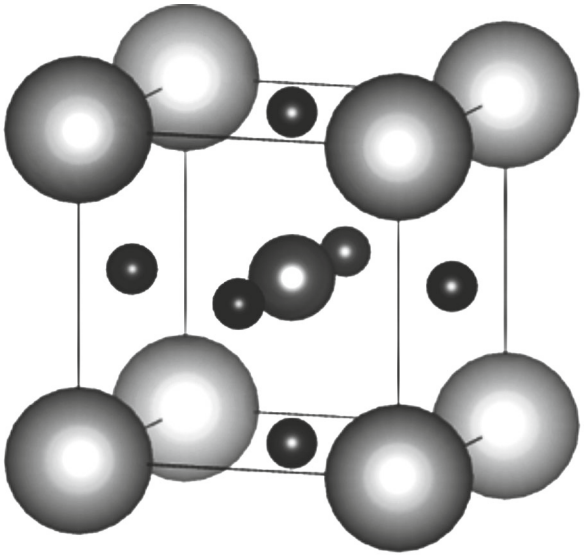

Fig. 1. Structure of perovskite $SrMO_3$. Large balls stand for Sr atoms; medium balls, for Fe and Mn atoms; and small balls, O atoms.

ization in thin $SrTiO_3$ films is well known [16, 17]. The substitution of a magnetic ion for a nonmagnetic ion would inevitably accompanied by the appearance of a magnetic order; in the presence of a ferroelectric phase, this substitution can cause the magnetoelectric effect, which is of obvious applied interest. Therefore, in this work, we studied $SrMO_3$ (M = Fe, Mn) oxides with a perovskite structure. It is experimentally known that a bulk $SrMnO_3$ crystal undergoes the G-type antiferromagnetic ordering at $T_N \approx 233$–260 K [18–20]. A spiral spin structure was detected in $SrFeO_3$ crystals, and the magnetic ordering changes into ferromagnetic ordering as the lattice parameter decreases [21–23]. However, unlike bulk compounds, the data on the polarization and magnetic properties of thin $SrMnO_3$ and $SrFeO_3$ films are scarce. As an example, we note the result [24], where the appearance of ferroelectricity in a thin $SrMnO_3$ film under the action of tensile stresses in the substrate was experimentally detected.

Table 1. Polar vibration mode frequency ν_{pol} and the calculated (a_{calc}) and experimental (a_{exp}) lattice parameters of bulk $SrMO_3$ (M = Mn, Fe) crystals

	$SrFeO_3$	$SrMnO_3$
a_{calc}, Å	3.86	3.89
a_{exp}, Å	3.85 [22]	3.86 [19]
ν_{pol}, cm^{-1}	131	21*i*

Therefore, the purpose of this work is to perform an ab initio investigation of the polarization, electronic, magnetic, and optical properties of bulk crystals and thin films of $SrMO_3$ perovskites containing magnetic ions.

2. CALCULATION PROCEDURE

All calculations were carried out using the VASP software package intended for ab initio computations and based on the density functional theory. For the calculations, we applied pseudopotentials, which were based on the projector augmented wave (PAW) method and used the Perdew–Burke–Ernzerhof (PBE) exchange-correlation potential with allowance for the generalized gradient approximation (GGA) [25, 26]. The following valence electron configurations were used for magnetic ions: $3p64s24d5$ for the Mn ion and $3p64s24d6$ for the Fe ion. To calculate the ground state, we applied the GGA + U approach in the Dudarev approximation [27], where $U' = U - J$ was taken to be 5 eV for both magnetic ions. All calculations were performed for spin-polarized states. Brillouin-zone integration was performed on the $6 \times 6 \times 6$ Monkhorst–Pack net [28] using the tetrahedron method. The plane wave cutoff energy was 500 eV. The lattice parameters and the atomic coordinates were optimized until the forces on atoms were lower than 0.02 eV.

3. RESULTS AND DISCUSSION

3.1. Bulk Crystals

Figure 1 shows the structure of perovskite $SrMO_3$, where M = Fe or Mn.

Table 1 gives the calculated and experimental lattice parameters of the crystals under study. The lattice parameter is seen to change within 1% when M cations are changed, and agreement with experiments is good (maximum difference is 3%). The dynamics of the crystal lattice of the bulk objects under study was calculated using the obtained equilibrium lattice parameters. Table 1 presents the determined frequencies of the low-frequency polar vibration modes for both compounds.

The calculation demonstrates that the ferroelectric mode in the bulk $SrFeO_3$ crystal is hard, indicating no ferroelectric phase transition in this compound, and $SrMnO_3$ has a small polar instability, which agrees with the results from [20].

To study the magnetic structure and the type of magnetic-moment ordering, we used the fourfold supercell (Fig. 2), which has lattice parameters $a' = \sqrt{2}a$, $b' = \sqrt{2}b$, and $c' = \sqrt{2}c$ and contains 20 atoms.

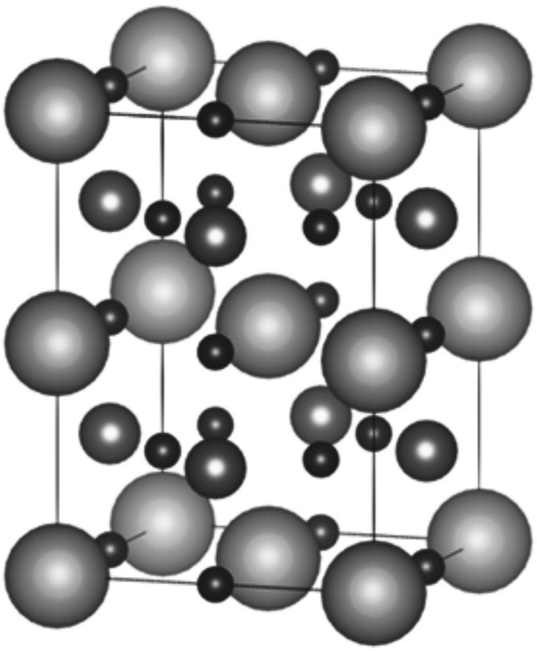

Fig. 2. Structure of the fourfold supercell containing 20 atoms. Large balls stand for Sr atoms; medium balls, for Fe and Mn atoms; and small balls, O atoms.

We considered the following cases of magnetic-moment ordering for each crystal: ferromagnetic ordering (*F*), antiferromagnetically coupled ferromagnetic planes (*A*), ferromagnetically coupled antiferromagnetic planes (*C*), and antiferromagnetic ordering in all planes (*G*) (Fig. 3). Geometry was optimized and the minimum energy was calculated for each version of magnetic ordering. Table 2 gives the calculation results.

As follows from Table 2, ferromagnetic ordering (*F*) for the $SrFeO_3$ crystal and *G*-type antiferromagnetic ordering for $SrMnO_3$ turned out to be most energetically favorable magnetic-moment ordering. The following two points are worth noting. First, the energies of the *A*-, *C*-, and *G*-type antiferromagnetic configurations in $SrMnO_3$ are close to each other. This calculation agrees with the results in [20], where the tension of an $SrMnO_3$ crystal was shown to induce additional magnetic transitions, first, to type *C* of antiferromagnetic ordering and, then, to type *A* of antiferromagnetic ordering. Second, as follows from the experimental data, the magnetic ordering in $SrFeO_3$ is related to the formation of a spiral spin structure [21, 22], which indicates competition between ferromagnetic and antiferromagnetic ordering. The nearest-neighbor exchange constant calculated with the SPR–KKR [29] software package is $J_1 = 1.4$ meV (which is close to the experimental value ($J_1 = 1.2$ meV)), a positive magnitude of which favors ferromagnetic magnetic-moment ordering. However, the next-nearest-neighbor exchange constant ($J_2 = -1.0$ meV) is negative, favors antiferromagnetic ordering, and is close to J_1. As follows from Table 2, the energies of the ferromagnetic phase and the antiferromagnetic phase (*A*) in $SrFeO_3$ are close, which is indirectly supported by the experimental data.

We also calculated the densities of states (DOS) of the most favorable magnetic configurations (Fig. 4). Both the *p* electrons of oxygen and the *d* electrons of Mn mainly contribute to the DOS at the Fermi level, and the *p* and *d* electrons of strontium weakly contribute to the total DOS and, hence, are not shown here. As follows from the occupancy of states at the Fermi level, all compounds under study are metals; however,

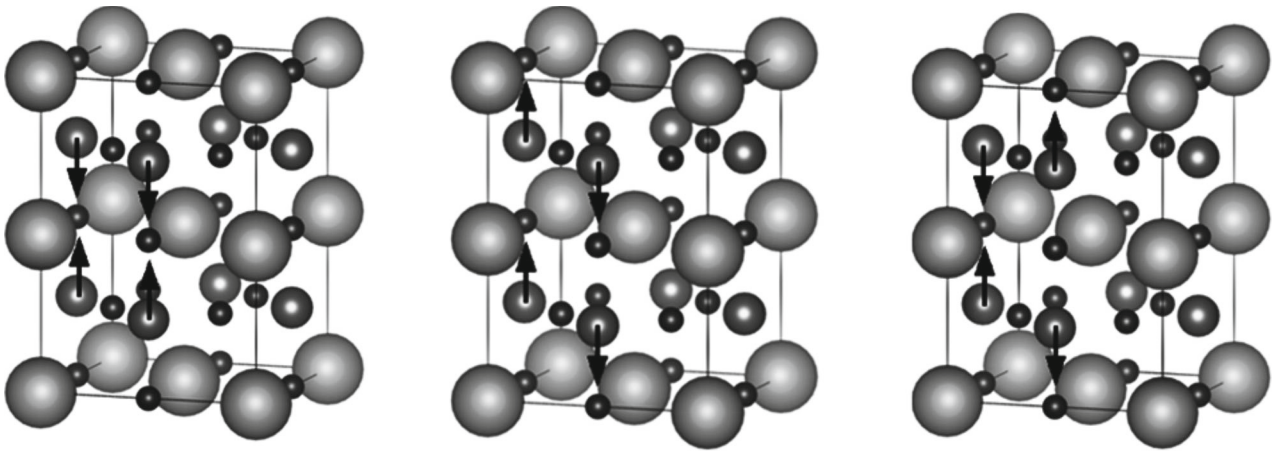

(a) (b) (c)

Fig. 3. Various types of antiferromagnetic magnetic-moment ordering in the compounds under study: (a) *A* type, (b) *C* type, and (c) *G* type. Large balls stand for Sr atoms; medium balls, for Fe and Mn atoms; and small balls, O atoms.

Table 2. Magnetic ordering configuration, total crystal energy E, and magnetic moment μ for bulk $SrFeO_3$ and $SrMnO_3$ crystals

	Type	E, eV	μ (Fe/Mn), μ_B
$SrFeO_3$	*F*-type	−139.183	2.871
	A-type	−138.918	±2.937
	C-type	−138.640	±2.917
	G-type	−138.225	±2.820
$SrMnO_3$	*F*-type	−147.317	2.664
	A-type	−147.542	±2.579
	C-type	−147.738	±2.547
	G-type	−147.845	±2.520

Table 3. Static conductivity δ_0/τ and plasma frequency ω_{pl} for bulk $SrFeO_3$ and $SrMnO_3$ crystals

	$SrFeO_3$	$SrMnO_3$
ω_{pl}, eV	10.436	0.5
δ_0/t, MS/m	0.21	0.01

Table 4. Polar vibration mode frequency ν_{pol} as a function of the substrate-induced misfit stress for thin $SrFeO_3$ and $SrMnO_3$ films

Misfit stress, %	ν_{pol}, cm^{-1}	
	$SrMnO_3$	$SrFeO_3$
−6	204	251
−4	177	227
−2	126	181
0	58	179
2	54*i*	87
4	73*i*	17
6	112*i*	14*i*

a dip in the DOS at the Fermi level of $SrMnO_3$ is worth noting. Low values of static electrical conductivity and plasma frequency in this compound in comparison with $SrFeO_3$ should also be noted (see Table 3). The presence of a peak, which is almost completely related to the *d* electrons of Fe at the Fermi level, is important; as a result, the spin polarization in these compounds is high.

The optical properties of a substance (refractive index n, extinction ratio k, loss function L, reflection coefficient R) are related to the dispersion dependence of permittivity $\varepsilon(\omega)$. We calculated the dispersion dependences of the real and imaginary parts of the permittivity of bulk $SrFeO_3$ and $SrMnO_3$ crystals for the most energetically favorable magnetic configurations (Fig. 5). The peaks in the imaginary part of the dielectric function correspond to the interband transitions induced by the passage of electrons from occupied states below the Fermi energy to empty states above the Fermi energy during light absorption. This relation can easily be traced by comparing the peaks in Fig. 5b with the DOS in Fig. 4. For example, a high-intensity peak exists in the imaginary part of the permittivity at an energy of about 2 eV (see Fig. 5b). At the same time, the DOS near the Fermi energy in Fig. 4 has two peaks, which are about 1 eV above and 1 eV below the Fermi energy, and the difference between them is about 2 eV.

3.2. Thin Films

As was noted in the previous section, the bulk crystals of the compounds under study do not have ferroelectric properties. Therefore, we now study the lattice dynamics of thin films of various thicknesses of these compounds to find how a decrease in the dimension and the stresses in a substrate affect their ferroelectric, magnetic, electronic, and optical properties. It should be noted that the appearance of ferroelectricity in a thin $SrMnO_3$ film was experimentally detected in [24]. To the best of our knowledge, there are no ab initio calculations for thin $SrMnO_3$ films.

To take into account the influence of the substrate-induced stresses, we reduced the effect of a substrate to the stress caused by the difference between the lattice parameters of an initial film and the substrate. The calculation results are given in Table 4.

As follows from Table 4, the polar mode in the phonon vibration spectra of thin $SrFeO_3$ and $SrMnO_3$ films is "hard" at an equilibrium lattice parameter. However, as the lattice parameter increases (i.e., when the mechanical tensile stress of the substrate is operative), the polar mode gradually becomes softer. In a thin $SrFeO_3$ film, the polar mode becomes "soft" at a high stress created by the difference between the lattice parameters of the film and the substrate. In a thin $SrMnO_3$ film, the polar mode becomes soft at a relatively low tensile stress (about 2%) and has a relatively high negative frequency squared, which indicates the appearance of a ferroelectric instability in the thin $SrMnO_3$ film.

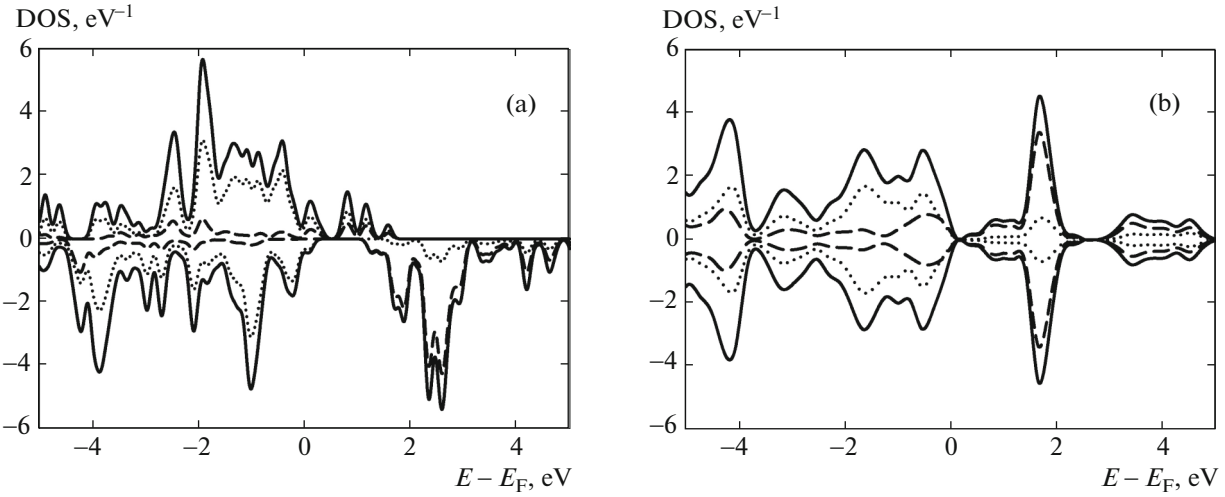

Fig. 4. Total and partial DOSs for (a) $SrFeO_3$ and (b) $SrMnO_3$. (solid curve) Total DOS, (dashed curve) *d* states of iron, and (dotted curve) *p* states of oxygen. Zero energy corresponds to the Fermi energy.

To study the types of magnetic ordering, we used a film, which contained three layers and was enlarged by four times in the film plane. Figure 6 schematically shows the analyzed cases of ordering the magnetic moments of Mn and Fe ions in thin films.

As a result of calculations, we found the minimum energies and the magnetic moments of various magnetic configurations in thin $SrFeO_3$ and $SrMnO_3$ films (see Table 5).

It is seen from Table 5 that, as in the bulk crystals, ferromagnetic magnetic-moment ordering (*F*) is energetically favorable for a thin $SrFeO_3$ film and the *G*-type magnetic-moment ordering is favorable for $SrMnO_3$. DOSs were calculated for the energetically favorable magnetic structures (see Fig. 7).

Table 5. Magnetic configuration, total energy *E*, and magnetic moment μ for thin $SrFeO_3$ and $SrMnO_3$ films

	Type of magnetic ordering	*E*, eV	μ (Fe/Mn), μ_B
$SrFeO_3$	*F*	−300.112	3.809
	A	−299.881	±3.809
	B	−299.184	±3.760
	C	−299.486	±3.759
	G	−298.917	±3.737
$SrMnO_3$	*F*	−315.033	3.190
	A	−315.015	±3.166
	B	−315.098	±3.140
	C	−315.137	±3.166
	G	−315.292	±3.135

As is seen in Fig. 7, a thin $SrFeO_3$ film is a ferromagnetic metal, as the corresponding bulk crystal. However, in contrast to the bulk crystal, a peak fully related to positive-spin electrons appears at the Fermi level; that is, 100% spin polarization of electrons appears in the film, which is interesting for spintronic applications. Unlike the bulk crystal, a thin $SrMnO_3$ film has a 1.5-eV energy gap; that is, $SrMnO_3$ undergoes a metal–insulator transition when going from the bulk to the thin-film state. Table 6 presents the static conductivities and plasma frequencies calculated for thin $SrFeO_3$ and $SrMnO_3$ films. It is seen that, although $SrFeO_3$ retains metallic properties in the thin-film state, its conductivity decreases significantly.

Only the *eg* electrons of iron mainly contribute to the DOS of $SrFeO_3$ near the Fermi level, and they also make a contribution to the spin polarization of this compound (Fig. 8a). The valence band in $SrMnO_3$ is occupied by both the *eg* and (predominantly) *t2g* electrons of manganese, and the conduction band is mainly formed by the unfilled *eg* states of Mn (Fig. 8b).

Thus, since a thin $SrMnO_3$ film is dielectric, a ferroelectric phase can appear in it during the condensation of the unstable polar mode (see Table 4). The polarization in the polar phase was calculated by the formula

$$P_\alpha = \frac{1}{V}\sum Z_{\alpha\beta}u_\beta,$$

where $Z_{\alpha\beta}$ are the dynamic Born charges and u_β is the displacement of ions in the low-symmetry phase with

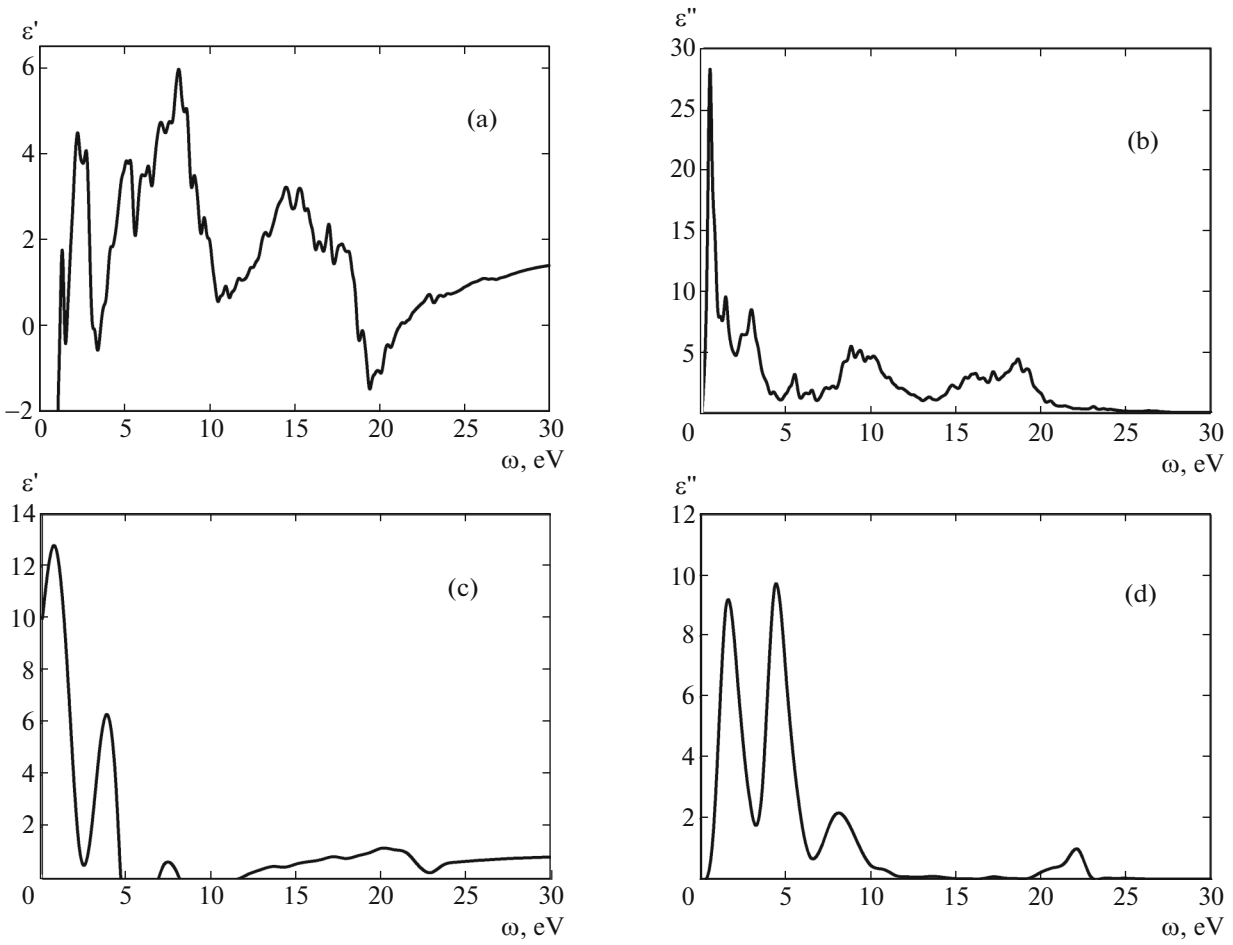

Fig. 5. Dispersion curves of the real and imaginary parts of the permittivity of (a, b) $SrFeO_3$ and (c, d) $SrMnO_3$.

respect to the high-symmetry phase; it was found to be $P = 23$ μC/cm^2. The results obtained agree qualitatively with the experimental observation of ferroelectric polarization in a thin $SrMnO_3$ film [24].

Finally, Fig. 9 depicts the dispersion dependences of the dielectric functions of thin $SrFeO_3$ and $SrMnO_3$ films. The dispersion components of the *xx* and *zz* components of the optical characteristics are seen to differ in the peak intensity, and the positions of the peaks almost coincide. The strong peaks in the imaginary part of the dielectric function of $SrMnO_3$ at an energy of 1.5 eV can be attributed to an electron transition from the valence band near the Fermi energy to the conduction band, which is separated by an energy gap of approximately the same value (Fig. 9d). The second peak at 4.5 eV can be related to a transition from the filled states near the Fermi energy to the empty *t2g* states, where DOS has a significant peak.

The difference between the optical properties of the bulk crystals and the thin films consists in, first, line broadening in the dispersion dependence of the

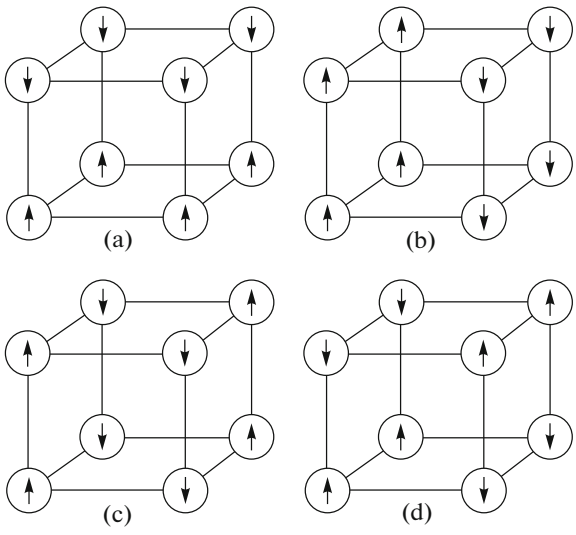

Fig. 6. Schematic images of the types of antiferromagnetic structures in thin $SrMO_3$ films: (a) *A* type of magnetic-moment ordering, (b) *B* type of antiferromagnetic ordering, (c) *C* type of antiferromagnetic ordering, and (d) *G* type of antiferromagnetic ordering.

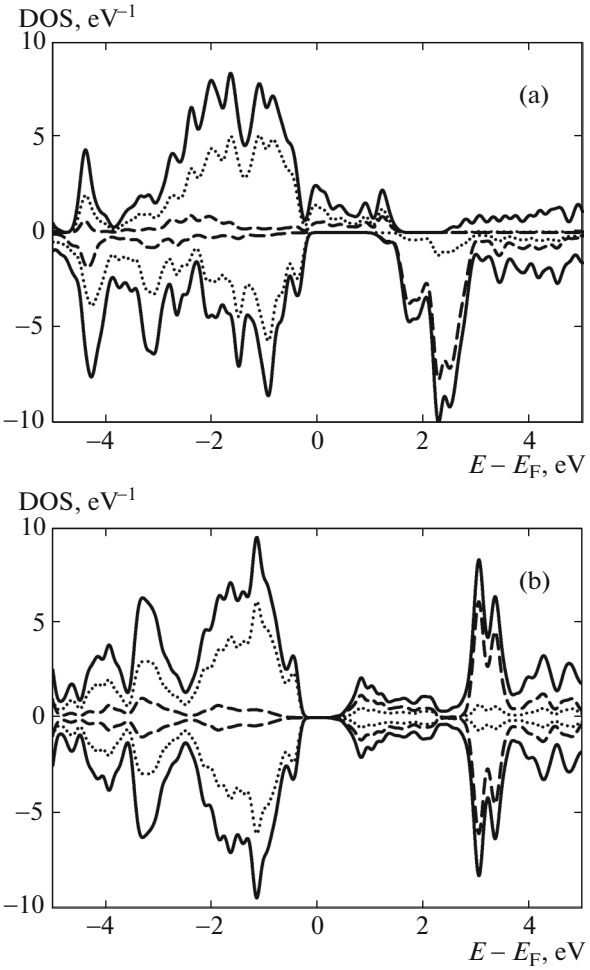

Fig. 7. Total and partial DOSs for (a) ferromagnetic $SrFeO_3$ phase and (b) antiferromagnetic *G* phase $SrMnO_3$. (solid curve) Total DOS, (dashed curve) *d* states of iron, and (dotted curve) *p* states of oxygen. Zero energy corresponds to the Fermi energy.

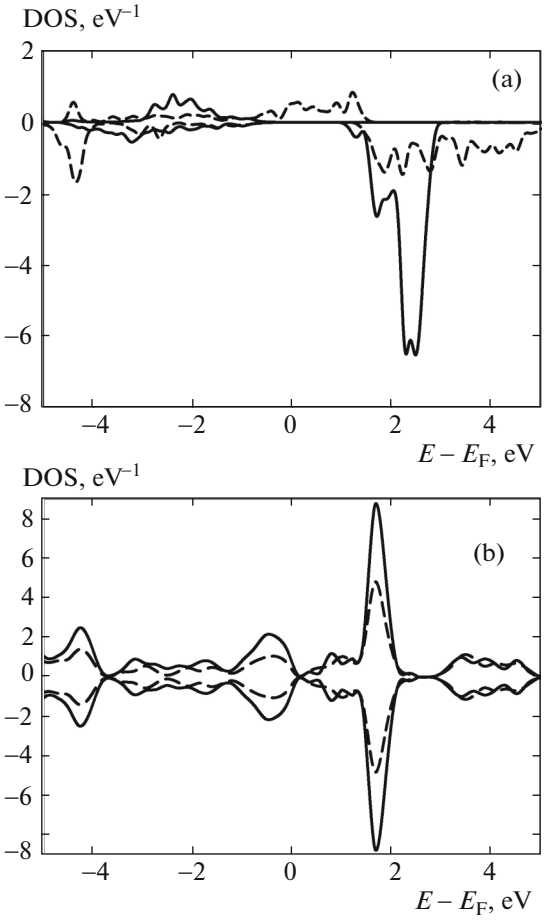

Fig. 8. DOS for (a) $SrFeO_3$ and (b) $SrMnO_3$. (solid curve) *t2g* electrons of manganese and (dashed curve) *eg* electrons of manganese. Zero energy corresponds to the Fermi energy.

dielectric function and, second, the appearance of new peaks, which are associated with a change in the electronic structure, in the central frequency range.

4. CONCLUSIONS

Using the density functional theory and the VASP software package, we studied the polarization, magnetic, electronic, and optical properties of bulk crystals and thin films of perovskite compounds containing magnetic ions and obtained the following results.

Bulk $SrFeO_3$ and $SrMnO_3$ crystals do not have ferroelectric instability. Ferroelectric instability is also absent in the corresponding thin films at an equilibrium lattice parameter; however, the polar vibration mode becomes softer as the substrate-induced tensile stresses grow.

Ferromagnetic ordering (*F*) in $SrFeO_3$ and *G*-type antiferromagnetic ordering in $SrMnO_3$ are most energetically favorable for both their bulk crystals and thin films. The bulk crystals of the compounds and a thin $SrFeO_3$ film are metals, whereas an energy gap with a width of about 1.5 eV appears in the DOS of a thin $SrMnO_3$ film. Along with the presence of a ferroelectric instability, this fact indicates the appearance of a ferroelectric phase in the thin film, which was supported by experimental data. Unlike the bulk crystal, a

Table 6. Static conductivity δ_0/τ and plasma frequency ω_{pl} for thin $SrFeO_3$ and $SrMnO_3$ films

	$SrFeO_3$		$SrMnO_3$	
	$x = y$	z	$x = y$	z
ω_{pl}, eV	2.42	0.98	0.00	0.0
δ_0/τ, MS/m	0.05	0.01	0.00	0.00

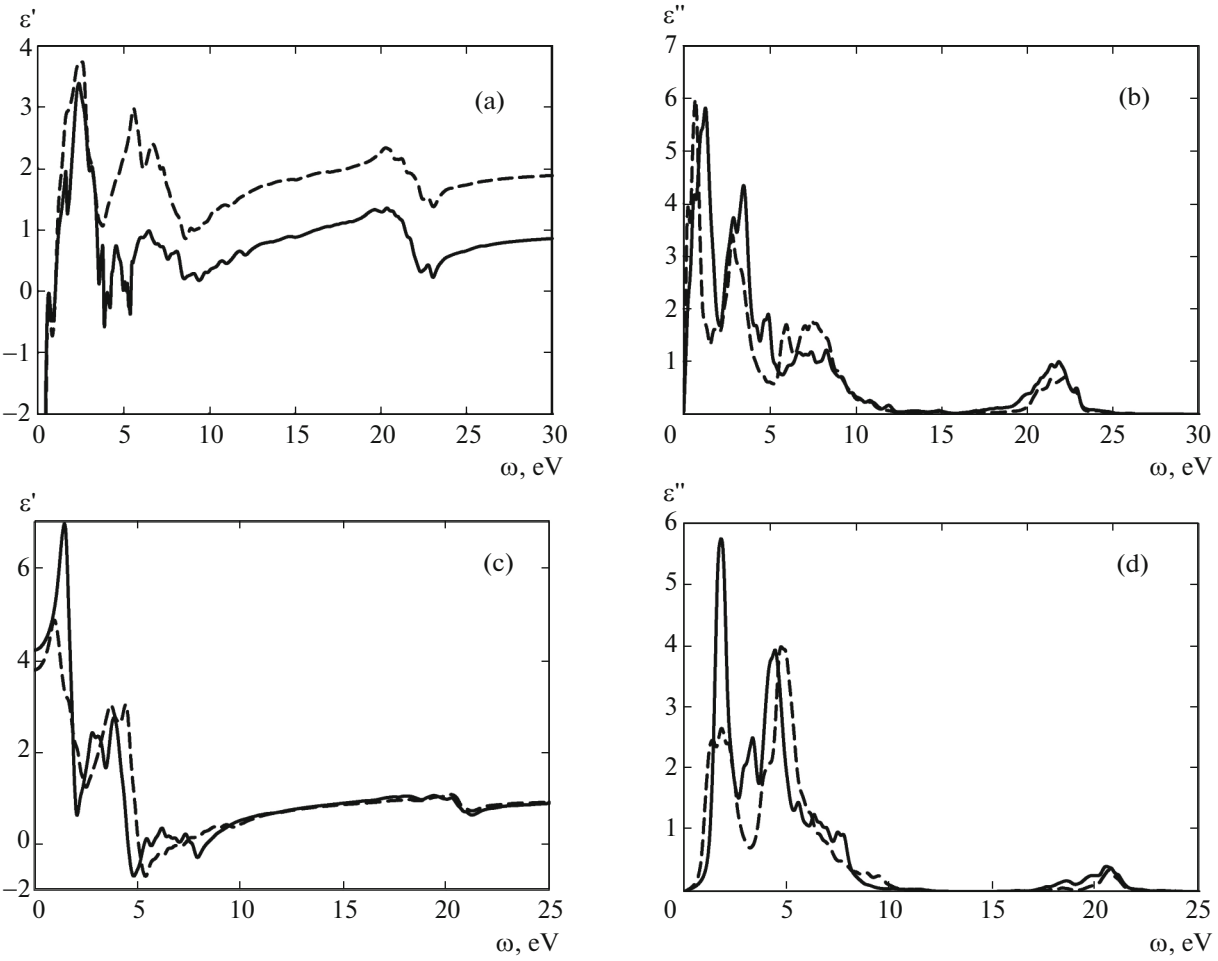

Fig. 9. Dispersion dependences of the real and imaginary parts of the permittivity of (a, b) $SrFeO_3$ and (c, d) $SrMnO_3$. (solid curve) *xx* component and (dashed curve) *zz* component.

thin $SrFeO_3$ film has 100% spin polarization, which makes it promising for spintronic applications.

The optical properties of the bulk crystals and the thin films of the compounds under study were calculated. The dispersion dependences of the optical properties in the bulk and thin-film states were determined and compared when the dimension of the system was reduced.

ACKNOWLEDGMENTS

The work was carried out using the computer abilities of the Collective Use Center "Complex Simulation and Data Processing of Mega-Class Experimental Setups" of the National Research Center "Kurchatov Institute," http://ckp.nrcki.ru.

This work was supported by the Russian Foundation for Basic Research (project no. 15-02-00340), the Government of the Krasnoyarsk Krai, and the Krasnoyarsk Krai Foundation for Support of Scientific and Research Activity (project no. 16-42-243035).

REFERENCES

1. Y. Bai, L. Han, X. Liu, X. Deng, X. Wu, C. Yao, Q. Liang, and J. Meng, J. Solid St. Chem. **217**, 64 (2014).
2. D. G. Franco, R. E. Carbonio, and G. Nieva, IEEE Trans. Magn. **49**, 4594 (2013).
3. G. Vaitheeswaran, V. Kanchana, and A. Delin, Appl. Phys. Lett. **86**, 032513 (2005).
4. D. Stoeffler and C. Etz, J. Phys.: Condens. Matter **18**, 11291 (2006).
5. S. Gong, P. Chen, and B. G. Liu, J. Magn. Magn. Mater. **349**, 74 (2014).
6. T. G. King, M. E. Preston, B. J. M. Murphy, and D. S. Cannell, Precis. Eng. **12**, 131 (1990).
7. H. Amorín, M. Algueró, R. del Campo, E. Vila, P. Ramos, M. Dollé, Y. Romaguera-Barcelay, J. Pérez de la Cruz, and A. Castro, Sci. Technol. Adv. Mater. **16**, 016001 (2015).
8. J. D. P. Rao and V. Krichevsky, IEEE Trans. Antennas Propag. **47**, 458 (1999).
9. A. Narazaki, K. Tanaka, and K. Hirao, J. Mater. Res. **14**, 3640 (1999).

10. J. F. Scott and C. A. P. D. Araujo, Science **246**, 1400 (1989).
11. R. Ramesh and N. A. Spaldin, Nat. Mater. **6**, 21 (2007).
12. Ni Hu, Chengliang Lu, Zhengcai Xia, RuiXiong, Pengfei Fang, Jing Shi, and Jun-Ming Liu, ACS Appl. Mater. Interfaces **7**, 26603 (2015).
13. L. W. Martin, S. P. Crane, Y.-H. Chu, M. B. Holcomb, M. Gajek, M. Huijben, C.-H. Yang, N. Balke, and R. Ramesh, J. Phys.: Condens. Matter **20**, 434220 (2008).
14. K. A. Müller and H. Bukard, Phys. Rev. B **19**, 3593 (1979).
15. W. Zhong and D. Vanderbilt, Phys. Rev. B **53**, 5047 (1996).
16. H. W. Jang, A. Kumar, S. Denev, et al., Phys. Rev. Lett. **104**, 197601 (2010).
17. J. H. Haeni, P. Irvin, W. Chang, R. Uecker, P. Reiche, Y. L. Li, S. Choudhury, W. Tian, M. E. Hawley, B. Craigo, A. K. Tagantsev, X. Q. Pan, S. K. Streiffer, L. Q. Chen, S. W. Kirchoefer, J. Levy, and D. G. Schlom, Nature (London, U.K.) **430**, 758 (2004).
18. O. Chmaissem et al., Phys. Rev. B **64**, 134412 (2001).
19. T. Takeda and S. Ohara, J. Phys. Soc. Jpn. **37**, 275 (1974).
20. J. H. Lee and K. M. Rabe, Phys. Rev. Lett. **104**, 207204 (2010).
21. T. Takeda, Y. Yamaguchi, and H. Watanabe, J. Phys. Soc. Jpn. **33**, 967 (1972).
22. Z. Li, T. Iitaka, and T. Tohyama, Phys. Rev. B **86**, 094422 (2012).
23. I. R. Shein, K. I. Shein, V. L. Kozhevnikov, and A. L. Ivanovskii, Phys. Solid State **47**, 2082 (2005).
24. C. Becher, L. Maurel, U. Aschauer, M. Lilienblum, C. Magén, D. Meier, E. Langenberg, M. Trassin, J. Blasco, I. P. Krug, P. A. Algarabel, N. A. Spaldin, J. A. Pardo, and M. Fiebig, Nat. Technol. **10**, 661 (2015).
25. G. Kresse and J. Furthmuller, Phys. Rev. B **54**, 11169 (1996).
26. J. P. Perdew, K. Burke, and M. Ernzerhof, Phys. Rev. Lett. **77**, 3865 (1996).
27. S. L. Dudarev, G. A. Botton, S. Y. Savrasov, C. J. Humphreys, and A. P. Sutton, Phys. Rev. B **57**, 1505 (1998).
28. H. J. Monkhorst and J. D. Pack, Phys. Rev. B **13**, 5188 (1976).
29. H. Ebert et al., The Munich SPR-KKR Package, Version 6.3. http://ebert.cup.uni-muenchen.de/SPRKKR; H. Ebert, D. Kodderitzsch, and J. Minär, Rep. Prog. Phys. **74**, 096501 (2011).

Translated by K. Shakhlevich